Dielectronic recombination and excitation autoionization rate coefficients for potassiumlike Mo^{23+} to fluorinelike Mo^{33+}

K. B. Fournier,* M. Cohen,† W. H. Goldstein, and A. L. Osterheld
Lawrence Livermore National Laboratories, Livermore, California 94551

M. Finkenthal† and M. J. May
Department of Physics and Astronomy, The Johns Hopkins University, Baltimore, Maryland 21218

J. L. Terry, M. A. Graf, and J. Rice
Plasma Fusion Center, Massachusetts Institute of Technology, Cambridge, Massachusetts 02139
(Received 11 March 1996; revised manuscript received 24 May 1996)

Fully relativistic, *ab initio* calculations of the rate of dielectronic recombination (DR) have been performed for fluorinelike Mo^{33+} to magnesiumlike Mo^{30+} and chlorinelike Mo^{25+} and argonlike Mo^{24+}. Calculations of the rate of excitation autoionization (EA) have been performed for neonlike Mo^{32+} to aluminumlike Mo^{29+} and argonlike Mo^{24+} and potassiumlike Mo^{23+}. The detailed calculations of the atomic structure and rate coefficients for charge states in these groups allow interpolation of the DR and EA rates for the more complex ions having $3s^2 3p^k$ ($k=1$–4 for DR and $k=2$–5 for EA) ground states. The calculations for DR are broken up by different classes of excitation channels; simple, analytic formulas are then fit to the calculations. The effects of configuration interaction on the rates of DR and EA have been studied in detail and are found to have a slight effect on only a small class of the Auger rates needed for the present work. Radiative transitions between energy levels in the continuum are investigated and found to have a moderate effect on the DR rates and a small effect on the EA rates of the ions in this paper. [S1050-2947(96)03211-8]

PACS number(s): 31.15.Ar, 34.80.Dp, 32.80.Dz

I. INTRODUCTION

The presence of impurities in a magnetically confined fusion plasma is unavoidable; vacuum vessel facing components and limiters contribute to the total concentration of high-Z ($Z>20$) impurities [1]. The presence of high-Z impurities can massively disrupt a fusion plasma through the power lost from ion line radiation [2] or through the effects on the plasma current profiles and spatial distribution of particles [3,4]. On the other hand, proposed schemes for controlling the rate at which impurities are sputtered from a reactor's wall into a fusion plasma, and for controlling the plasma heat flux onto the reactor's divertor strike plates call for the controlled introduction of high-Z atoms for use as radiative ''coolants'' [5]. Whether one tries to prevent the deleterious effects of impurities on plasma power balance or use them as edge coolants in a reactor, accurate models of the distribution of ionization states in the plasma are necessary.

The motivation for the present calculations comes from the observation of significant differences between measured radial molybdenum ion distributions in the Alcator C-Mod tokamak (Plasma Fusion Center, Massachusetts Institute of Technology) and predictions made with a plasma modeling code which relies on an average-atom model [6] of atomic processes (these observations are discussed in a companion paper by Rice *et al.* [7]). For instance, Fig. 1 shows the radial distribution of the measured brightness of a $2p_{3/2}$-$4d_{3/2}$ transition (at 3717.8 mÅ) in F I-like Mo^{33+} and a $2p_{3/2}$-$4d_{5/2}$ transition (at 3785.7 mÅ) in Na I-like Mo^{31+}. For each tran-

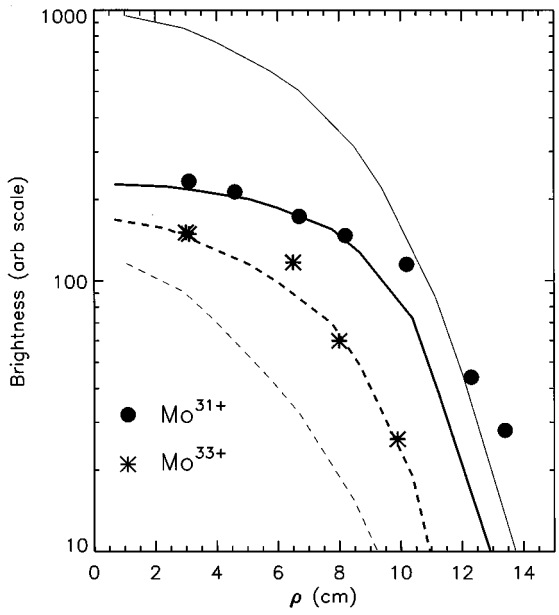

FIG. 1. $2p_{3/2}$-$4d_{3/2}$ Mo^{33+} and $2p_{3/2}$-$4d_{5/2}$ Mo^{31+} line brightness as measured in the Alcator C-Mod tokamak and predicted using measured temperature and density profiles, the MIST plasma transport code [8], and average-atom atomic physics (thin lines) and the same model with the atomic physics data of the present work (thick lines).

*Permanent address: The Johns Hopkins University, Baltimore, MD 21218.

†Permanent address: Racah Institute of Physics, Hebrew University, Jerusalem, Israel.

sition, there are two curves in the figure which are the predicted spatial brightness profile using a model based on (thin line) the MIST transport code (written by Hulse at the Princeton Plasma Physics Laboratory) [8], average-atom atomic physics [6], and measured T_e and n_e radial profiles, and (thick line) the same plasma model [8] and measured temperature and density profiles, and the atomic data in the present work. The model with the present ionization and recombination data achieves agreement with the experimental data for both charge states. The excitation mechanisms of the observed lines and measured plasma transport properties are discussed in detail in paper by Rice *et al.* [7].

The agreement between theory and experiment in Fig. 1 is obtained when the dielectronic recombination (DR) and electron-impact excitation followed by autoionization (EA) processes, as treated in the present paper, are introduced into the calculation of the distribution of Mo ionization states. For high-temperature plasmas, it is known that DR is one of the most significant recombination processes [9,10]. Burgess originally provided a semiempirical formula [9] which accounted for the important DR process, and which was later made more general by Merts, Cowan, and Magee for ions from atoms up to iron ($Z=26$) [11]. In recent years, a great deal of effort has gone into calculating detailed DR rates for highly ionized, heavy elements. The complexity of this task, which is due to the tremendous number of intermediate states through which the recombined ion may pass, has meant that the work has been confined mainly to isosequences with simple ground-state configurations such as the sodiumlike isosequence [12,13], the neonlike isosequence [14–17], and the fluorinelike isosequence [18–20]. The neonlike and fluorinelike isosequences (including Mo^{32+} and Mo^{33+}) have been treated by Chen in Refs. [14,18]; the works there are closely related to this paper in that they contain fully relativistic, *ab initio* calculations of the DR rate coefficient. Recently, analytic formulas from fits to Chen's data for fluorinelike ions have been published [21]. LS-coupled calculations for the rates of DR in sodiumlike ions [12,13] and in magnesiumlike ions [22,23] have been performed without considering wave-function mixing. The results of these calculations have been collected by Hahn [24] and used in generating analytical formulas for dielectronic recombination rate coefficients. As will be seen below, the detailed accounting of energy levels and relativistic calculations of transition rates in the present work result in an enhancement of DR rates over configuration-average, nonrelativistic models.

Ionization physics is greatly altered by multistep processes; previous work has shown that for simple isosequences such as lithiumlike and sodiumlike ions, excitation autoionization can enhance the total ionization rate for an ion by factors of 2 or 3 [25–28]. EA effects in atoms lighter than molybdenum have been studied for charge states near neonlike as this isosequence is important in x-ray laser schemes [29,30]. Calculations of EA rates done with the same atomic structure codes that are used in this paper have been performed for the galliumlike isosequence [31,32] of rare earth ($Z=59$–70) elements and for zinclike molybdenum [33]. Recently a thorough calculation of EA rates for N-shell isosequences of high-Z elements through the $3d^9 4s^m 4p^n 4d$ and $3d^9 s^m 4p^n 4f$ ($m \leqslant 2$, $n \leqslant 6$) manifolds and a comparison of those rates to ground-state collisional ionization rates has been published [34].

Presented below are detailed calculations for the rate coefficients of the processes of DR (Sec. II) for fluorinelike Mo^{33+} to magnesiumlike Mo^{30+} and chlorinelike Mo^{25+} and argonlike Mo^{24+} and EA (Sec. III) for neonlike Mo^{32+} to aluminumlike Mo^{29+} and argonlike Mo^{24+} and potassiumlike Mo^{23+}. Our calculations use a fully relativistic structure code and detailed accounting of level energies to derive the rate coefficients. For the remaining intermediate charge states, Mo^{26+} to Mo^{29+} for DR and Mo^{25+} to Mo^{28+} for EA, rate coefficients are generated (in Sec. IV) from analytic formulas determined by fits to the calculated data in Secs. II and III.

II. DIELECTRONIC RECOMBINATION

A. Calculation of dielectronic recombination rate coefficients

The dielectronic recombination process can be illustrated with some generality using the case of (Na I-like) Mo^{31+}. Recombination from the ground state is allowed to proceed in the present work through

$$\begin{aligned}(2s^2 2p^6 3s) + e^- &\rightarrow (2s2p^6 3sn'l'n''l'' + 2s^2 2p^5 3sn'l'n''l'' \\ &\quad + 2s^2 2p^6 n'l'n''l'') \\ &\rightarrow (2s^2 2p^6 nln^*l^* + h\nu), \end{aligned} \tag{1}$$

where the final state (either singly or doubly excited) lies below the ionization potential of Mo^{30+}. The recombined, doubly excited states in Eq. (1) are formed by the capture of the free electron and a $2l \rightarrow 3l'$, $3l \rightarrow 3l'$, or $3l \rightarrow 4l'$ excitation. The $\Delta n = 2$ excitations of bound electrons (e.g., $2l \rightarrow 4l'$) have been found to contribute a negligible amount to the total DR rate for all the isosequences considered here. The present calculations are performed in the zero-density regime and in the isolated-resonance approximation. This means, first, that possible collisional quenching via electron impacts of radiative stabilization channels from the intermediate, doubly excited states is not taken into account, and only ground initial states are considered. For low-density ($\sim 10^{14}$ cm^{-3}) tokamak plasmas, this is reasonable. The best confirmation of this assumption is the agreement with the experiment as discussed in the last section. Second, only limited configuration interaction (CI) is included in the calculation. (Details about how CI is included in the wave functions of the recombined ions will be given in the discussion below.)

The rate of DR for some ion with charge $q+$ into the adjacent ionization state, charge $(q-1)+$, can be described in the isolated-resonance approximation as a function of electron temperature T_e by

$$\alpha_i^{\mathrm{DR}}(T_e) = \sum_j V_j(T_e)\omega_j, \tag{2}$$

where i is an energy level of initial ion $q+$, j is an energy level of ion $(q-1)+$ above the ionization limit, $V_j(T_e)$ is the electron capture probability in cm^3 sec^{-1}, and ω_j is the

branching ratio for radiative stabilization from level j. The capture probability can be expressed as

$$V_j(T_e)=\frac{g_j A^a_{j,i}}{2g_i}\left(\frac{4\pi R a_0^2}{T_e}\right)^{3/2}\exp(-\Delta E_{j,i}/T_e), \quad (3)$$

where g is the multiplicity of a given level, $A^a_{j,i}$ is the autoionization rate coefficient, R is the Rydberg unit of energy, $\Delta E_{j,i}$ is the capture energy of the free electron, and a_0 is the Bohr radius. The branching ratio for radiative stabilization is

$$\omega^c_j=\frac{1}{\Gamma_j}\left[\sum_f\left\{A^r_{j,f}+\sum_{j'}\frac{A^r_{j,j'}}{\Gamma_{j'}}\left(A^r_{j',f}+\sum_{j''}\frac{A^r_{j',j''}}{\Gamma_{j''}}\times(A^r_{j'',f}+\cdots)\right)\right\}\right], \quad (4)$$

where the states labeled f are stable against autoionization, and the states labeled $j',j'',\ldots$ are not, and where

$$\Gamma_j=\sum_f A^r_{j,f}+\sum_i A^a_{j,i}. \quad (5)$$

The sum over the Einstein coefficients in Eq. (5), that is, over the final states f of radiative decays from some level j, involves only states stable against autoionization; each Γ in Eq. (4) includes only radiative transitions to states below the continuum. For each state of the recombined ion in the continuum, j, other states in the continuum, j', are reachable by radiative transitions. Each term in the sum over j' in Eq. (4) tracks the probability for a transition between levels in the continuum to undergo a transition to a stable, bound state; thus the effect of cascades between levels belonging to the recombined ion lying in the continuum is included in the calculation of the recombination rate coefficient.

The possibility for a decay to a state below the continuum after each transition between levels in the continuum enhances the total width for radiative stabilization compared to a simpler calculation which only allows a level in the continuum to decay to states below the continuum. Hence the total DR rate for a given ion is enhanced. In the present work, we have allowed for two generations of cascades; this is expressed mathematically by the terms explicitly listed in Eq. (4). The branching ratio for subsequent autoionization from the lower state of many of the transitions between levels in the continuum is often quite large and the overall probability for stabilization of the recombined ion is only modestly enhanced ($\approx$5–15 %) by including radiative transitions in the continuum in the DR calculation. When transitions between levels in the continuum are ignored, the code which computes the DR rate coefficient for a particular manifold can run on a dedicated work station in a matter of minutes. With one generation of cascades, the code runs for hours on the same work station. For two generations of cascades, the memory requirements of the computer to compile the code, and the speed needed to complete the branching ratio calculation for the more complicated ions in a reasonable time are obtained on a Cray YMP computer at the National Energy Research Supercomputing Center (NERSC). Energy levels and transition probabilities have been calculated with the relativistic parametric potential code RELAC [35]. RELAC's method of computation of autoionization rates is described in detail in Ref. [33].

B. Overview of recombination channels

Three recombination channels are considered for the M-shell ions (Mo^{31+} to Mo^{24+}) in the present work: these are the L-shell $\Delta n=1$, M-shell $\Delta n=0$, and M-shell $\Delta n=1$ channels. For the L-shell ions (Mo^{33+} and Mo^{32+}) in the present work, there are no M-shell recombination channels from the ground configurations; for Mo^{33+}, with a single L-shell vacancy, an L-shell $\Delta n=0$ channel has also been considered. The recombination channels for M-shell ions are discussed below; radiative stabilization channels from intermediate states of the recombined ions are discussed in Sec. II C, below.

The dominant recombination channel at temperatures above 2 keV for the higher charge states of interest to the current work proceeds through electron capture accompanied by a $\Delta n=1$ excitation of a bound $n=2$ (L-shell) electron:

$$2l^8[\text{core}]+e\rightarrow 2l^7[\text{core}]n'l'n''l'', \quad (6)$$

where $2l$ can be either a $2s$ or $2p$ orbital and ''core'' represents a set of spectator electrons. For (Mg I-like) Mo^{30+} this would mean a capture plus excitation leading to a state of the form $2s2p^6 3s^2 3p4l$ or $2s^2 2p^5 3s^2 3d4l$; Table I lists all doubly excited manifolds in the recombined ions through which recombination has been allowed to proceed, as well as the final states for autoionization from the doubly excited states in the L-shell $\Delta n=1$ recombination channel. The intermediate manifolds of the L-shell $\Delta n=1$ recombination channel have been allowed to autoionize to all singly excited states of the initial ion with an electron in either an $n=3$ or 4 shell. Singly excited states with a valence electron in a shell with $n\geqslant 5$ are reachable by autoionization from the doubly excited manifolds of the recombined ion [that is, for Mo^{30+}, the intermediate $2s2p^6 3s^2 3p5l$ states can autoionize to the $2s^2 2p^6 3s5l$ states of the Mg I-like (initial) ion]; by neglecting these autoionizing transitions, we estimate the contribution to the DR rate through the L-shell $\Delta n=1$ channel from the manifolds with a captured electron in an $n''\geqslant 5$ shell may be too large by as much as 25%. The contribution of all doubly excited manifolds with $n''\geqslant 5$ is typically $\sim$35% of the total DR rate through the L-shell $\Delta n=1$ channel, hence the overestimate of the total DR rate for the L-shell $\Delta n=1$ channel is well under 20%.

Configuration interaction in the doubly excited intermediate states of the L-shell $\Delta n=1$ channel has been accounted for as fully as possible within computational limits. For each manifold of levels considered, all states formed by promotion of a $2l$ electron to all $3l'$ orbitals (with $l'=s$, p, and d as available) are allowed to interact (that is, in Mo^{30+} the $2s2p^6 3s^2 3p4l''$ and $2s^2 2p^5 3s^2 3d4l''$ states for all values of l'' are allowed to mix). The present calculations were run with and without CI between the states with a $2s$ hole and a $2p$ hole; it was found for the $n''=3$ manifolds of Mo^{30+} and Mo^{31+} that CI enhances some autoionization rates to excited states of the initial ion by nearly 20%. The effect of CI on higher manifolds is found to be rapidly diminishing as the centers of gravity of the states with a $2s$ hole and a $2p$ hole

TABLE I. Configurations used in computing the recombination rate coefficient through the L-shell $\Delta n=1$, M-shell $\Delta n=0$, and M-shell $\Delta n=1$ channels in Mo^{24+}, Mo^{25+}, Mo^{30+}, and Mo^{31+}. Also shown are final states for autoionization from the intermediate states of the recombined ions. n_0 indicates the first manifold of the M-shell $\Delta n=0$ channel to include levels which lie in the continuum.

	L-shell $\Delta n=1$
Excitation + capture channels:	$[2l^8]3s^m3p^k+e\rightarrow[2l^7]3s^m3p^k3l'n''l''$ (where $n''\leqslant15$, $l''\leqslant5$)
	Ar I-like Mo^{24+} $m=2$, $k=6$, $l'=d$
	Final autoionization states: $3s^23p^6$, $3s^23p^53d$, $3s3p^63d$, $3s^23p^54l(l\leqslant3)$
	Cl I-like Mo^{25+} $m=2$, $k=5$, $l'=p,d$
	Final autoionization states: $3s^23p^5$, $3s^23p^43d$, $3s3p^6$, $3s3p^53d$, $3s^23p^44l(l\leqslant3)$
	Mg I-like Mo^{30+} $m=2$, $k=0$, $l'=p,d$
	Final autoionization states: $3s3l(l\leqslant2)$, $3s4l(l\leqslant3)$
	Na I-like Mo^{31+} $m=1$, $k=0$, $l'=s,p,d$
	Final autoionization states: $3l(l\leqslant2)$, $4l(l\leqslant3)$
	M-shell $\Delta n=0$
Excitation + capture channels:	$3s^m3p^k+e\rightarrow3s^{m-1}3p^k3l'n''l''$ (where $n_0\leqslant n''\leqslant19$, $l''\leqslant5$) and $3s^m3p^k+e\rightarrow3s^m3p^{k-1}3l'n''l''$ (where $n_0<n''\leqslant19$, $l''\leqslant5$)
	Ar I-like Mo^{24+} $n_0=6$, $m=2$, $k=6$, $l'=d$
	Final autoionization states: $3s^23p^6$, $3s^23p^53d$, $3s3p^63d$
	Cl I-like Mo^{25+} $n_0=6$, $m=2$, $k=5$, $l'=p,d$
	Final autoionization states: $3s^23p^5$, $3s^23p^43d$, $3s3p^6$, $3s3p^53d$
	Mg I-like Mo^{30+} $n_0=8$, $m=2$, $k=0$, $l'=p,d$
	Final autoionization states: $3s3l(l\leqslant2)$
	Na I-like Mo^{31+} $n_0=9$, $m=1$, $k=0$, $l'=s,p,d$
	Final autoionization states: $3l(l\leqslant2)$
	M-shell $\Delta n=1$
Excitation + capture channels:	$3s^m3p^k+e\rightarrow3s^{m-1}3p^k4l'n''l''$ (where $l'\leqslant3$, $n''\leqslant12$,$l''\leqslant5$) and $3s^m3p^k+e\rightarrow3s^m3p^{k-1}4l'n''l''$ (where $l'\leqslant3$, $n''\leqslant12$,$l''\leqslant5$)
	Ar I-like Mo^{24+} $m=2$, $k=6$
	Final autoionization states: $3s^23p^6$, $3s^23p^53d$, $3s3p^63d$, $3s^23p^54l(l\leqslant3)$
	Cl I-like Mo^{25+} $m=2$, $k=5$
	Final autoionization states: $3s^23p^5$, $3s^23p^43d$, $3s3p^6$, $3s3p^53d$, $3s^23p^44l(l\leqslant3)$
	Mg I-like Mo^{30+} $m=2$, $k=0$
	Final autoionization states: $3s3l(l\leqslant2)$, $3s4l(l\leqslant3)$
	Na I-like Mo^{31+} $m=1$, $k=0$
	Final autoionization states: $3l(l\leqslant2)$, $4l(l\leqslant3)$

move farther apart with increasing n''. The electron capture rate for the $n''=3$ manifold in Mo^{30+} and Mo^{31+} [Eq. (3)] is enhanced by 5% when the full spectrum of CI effects in the autoionization rates from $n''=3$ levels is included; no effect from CI was observed for Mo^{25+} and Mo^{24+}. Figure 2 shows the DR rate through the L-shell $\Delta n=1$ channel for Mo^{24+}, Mo^{25+}, Mo^{30+}, and Mo^{31+} as a function of electron temperature. The rates estimated in Sec. IV for Mo^{26+} to Mo^{29+} are also shown.

The rate coefficients of dielectronic recombination through the L-shell $\Delta n=0$ and $\Delta n=1$ $2l^m+e\rightarrow2l^{m-1}n'l'n''l''$ channels for Mo^{33+} and Mo^{32+} have been computed. A comparison is made in Fig. 3 between the relativistic, parametric potential calculation (solid lines) of the present work and Chen's multiconfiguration Dirac-Fock (MCDF) calculation (long dashes) of the DR rate for Mo^{33+} (circles) and Mo^{32+} (squares). (Note, the different behaviors of the rate coefficients for Mo^{33+} and Mo^{32+} are a result of the L-shell $\Delta n=0$ excitation channel in Mo^{33+}, $2s^22p^5+e\rightarrow2s2p^6n''l''$.) Our calculation of the rate of recombination for fluorinelike molybdenum matches Chen's [18] to better than 2% at temperatures above 1 keV, and to better than 15% at temperatures near 1 keV. Our calculation of the neonlike molybdenum recombination rate agrees with Chen's [14] to better than 5% at temperatures above 1 keV, and to within 20% at temperatures of a few hundreds of

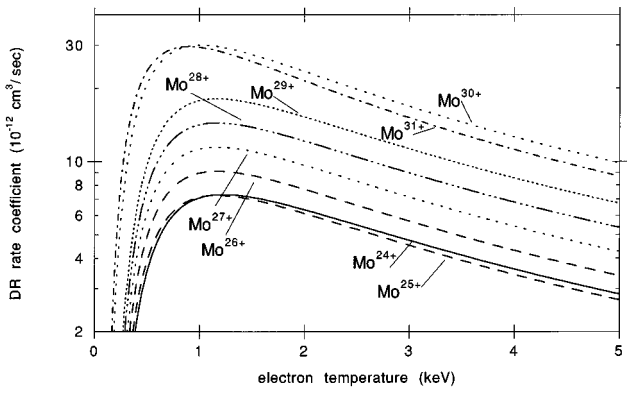

FIG. 2. DR rate coefficients for the L-shell $\Delta n=1$ channel between 50 and 5000 eV. The rate coefficients for Mo^{24+}, Mo^{25+}, Mo^{29+}, Mo^{30+}, and Mo^{31+} are explicitly calculated in Sec. II. The rate coefficients for Mo^{26+}, Mo^{27+}, and Mo^{28+} are generated by interpolation in Sec. IV.

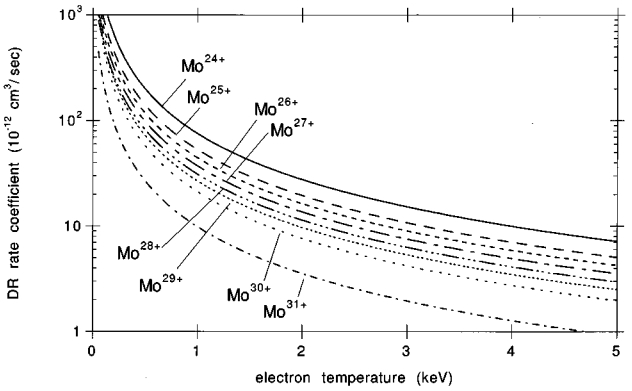

FIG. 4. DR rate coefficients for the M-shell $\Delta n=0$ channel between 50 and 5000 eV. The rate coefficients for Mo^{24+}, Mo^{25+}, Mo^{30+}, and Mo^{31+} are explicitly calculated in Sec. II. The rate coefficients for Mo^{26+}, Mo^{27+}, Mo^{28+}, and Mo^{29+} are generated by interpolation in Sec. IV.

electron volts. Comparisons between the codes used here [32,35] and the MCDF method used by Chen have also appeared elsewhere [33,36] and find agreement between calculated Auger transition rates and dielectronic recombination rates over a broad range of temperatures to within 5%. The comparisons in Refs. [33,36], made for neonlike iron, find that RELAC's DR rates are systematically larger than the MCDF calculated rates by about 15% at very low temperatures. Figure 3 also shows Roszman's nonrelativistic calculation (short dashes) of the total DR rate for Mo^{32+} [16].

The dominant recombination channel for the charge states of interest to the current work at temperatures below 1.5 keV proceeds via electron capture accompanied by an excitation of a bound $n=3$ (M-shell) electron of the form

$$[2l^8]3s^m3p^k+e\rightarrow[2l^8]3s^{m-1}3p^k3l'n''l'' \quad \text{or} \quad [2l^8]3s^m3p^{k-1}3l'n''l'', \qquad (7)$$

where $m=1$ or 2, $0\leqslant k\leqslant 6$, and $3l'$ can be either a $3p$ (if available) or $3d$ orbital. For example, in Mo^{25+} this channel proceeds through states of the form $[2l^8]3s^23p^43d9h$ and

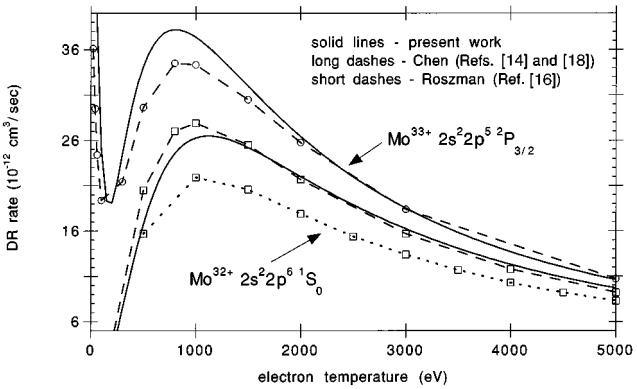

FIG. 3. RELAC's DR rates for Mo^{33+} and Mo^{32+} (solid lines) and previously published MCDF values from Refs. [14,18] (Mo^{33+} circles, dashes; Mo^{32+}, squares, dashes). Also shown is Roszman's (Ref. [16]) nonrelativistic calculation of the DR rate for Mo^{32+} (squares, short dashes).

$[2l^8]3s3p^69h$. The dominance of this channel at low electron temperatures is due to the small energy difference between the doubly excited state of the recombined ion and the ground state of the initial ion [$\Delta E_{j,i}$ in Eq. (3)]; the small energy difference causes the exponential term in Eq. (3) to start off large at low temperatures and rapidly fall off as T_e increases. The existence of $3p$ excitations in the M-shell $\Delta n=0$ channel for Ar I-like Mo^{24+} and Cl I-like Mo^{25+} means this channel is larger in these ions than in Mg I-like Mo^{30+} and Na I-like Mo^{31+}. The M-shell $\Delta n=0$ channel is the most tractable channel for computations in the present work. The first manifold of the recombined ion to lie in the continuum (that is, the first $3s+e\rightarrow 3dn_0''l''$ excitation and capture) is $n_0''=9$, 8, 7, 6, and 6 for each initial ion, Mo^{31+}, Mo^{30+}, Mo^{29+}, Mo^{25+}, and Mo^{24+}, respectively.

The doubly excited manifolds through which recombination was allowed to proceed, as well as the final states for autoionization from the doubly excited states in the M-shell $\Delta n=0$ channel of the recombined ion are listed in Table I. The doubly excited states for the M-shell $\Delta n=0$ channel in Table I converge to the excited states of the next higher ion, that is, in the M-shell $\Delta n=0$ channel for DR of Mo^{25+}, the recombined states $3s3p^53ln''l''$ will never lie above the $3s3p^53l$ states of the initial ion. Hence autoionization to excited states of the initial ion from the intermediate states of the recombined ion is completely accounted for. The contribution of the M-shell $\Delta n=0$ channel to the total DR rate coefficient as a function of electron temperature is shown in Fig. 4. The rates estimated in Sec. IV for Mo^{26+}, Mo^{27+}, and Mo^{28+} are also shown.

The M-shell $\Delta n=1$ recombination channel (electron capture accompanied by an excitation of a bound $n=3$ electron to an $n=4$ orbital) has a significant contribution to the total DR rate for the ions in the current work at all temperatures. Recombination in the M-shell $\Delta n=1$ channel proceeds through

$$[2l^8]3s^m3p^k+e\rightarrow[2l^8]3s^{m-1}3p^k4l'n''l'' \quad \text{or} \quad [2l^8]3s^m3p^{k-1}4l'n''l'', \qquad (8)$$

where $m=1$ or 2, $0\leqslant k\leqslant 6$, and $4l'$ can be any orbital in the

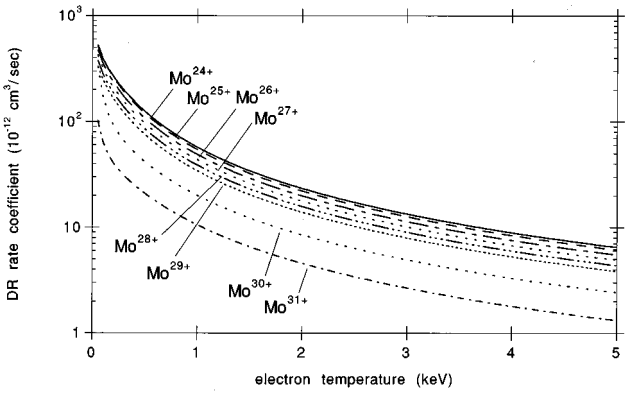

FIG. 5. DR rate coefficients for the M-shell $\Delta n=1$ channel between 50 and 5000 eV. The rate coefficients for Mo^{24+}, Mo^{25+}, Mo^{30+}, and Mo^{31+} are explicitly calculated in Sec. II. The rate coefficients for Mo^{26+}, Mo^{27+}, Mo^{28+}, and Mo^{29+} are generated by interpolation in Sec. IV.

N-shell with $l'\leqslant 3$. For example, in Mo^{25+} these capture plus excitation events can proceed through $3s^23p^5+e\rightarrow 3s3p^54p5g$ or $3s^23p^5+e\rightarrow 3s^23p^44d6f$. The DR rate coefficient through this channel starts off large at low electron temperatures and falls off in a manner similar to that of the M-shell $\Delta n=0$ channel due to the low excitation energies (compared to the electron temperatures in the present work) between some of the $3l$ bound orbitals and the $4s$ (and some $4p$) excited orbitals. The M-shell $\Delta n=1$ channel's contribution to the total rate coefficient is less at low temperatures than that of the M-shell $\Delta n=0$ channel and is comparable to that of the L-shell $\Delta n=1$ channel at high temperatures. Table I lists all doubly excited manifolds through which recombination was allowed to proceed, as well as the final states for autoionization from the intermediate states in M-shell $\Delta n=1$ channel. The contribution of the M-shell $\Delta n=1$ channel to the total DR rate coefficient as a function of electron temperature for Mo^{24+}, Mo^{25+}, Mo^{30+}, and Mo^{31+} is shown in Fig. 5. The rate coefficients estimated in Sec. IV for Mo^{26+} to Mo^{29+} are also shown.

A treatment of the M-shell $\Delta n=1$ channel which fully accounts for configuration interaction generates the largest amount of data per ion of all the channels considered in the present work. For Mo^{24+}, Mo^{30+}, and Mo^{31+}, all possible states formed by promoting a $3l$ electron to a $4l'$ orbital, for a fixed value of the principal quantum number of the captured electron, n'', are allowed to interact. For example, in Mo^{24+}, the $3s3p^64l'n''l''$ and $3s^23p^54l'n''l''$ states are computed with mixing between all values of $l'\leqslant 3$ and $l''\leqslant 5$. The calculation for the M-shell $\Delta n=1$ channel of Mo^{25+} was too large to be treated in the same manner. For Mo^{25+} the rate of recombination for each value of the orbital quantum number in the $4l'$ excited orbital was computed separately, that is, $3s^23p^5+e\rightarrow 3s3p^54pn''l''$ and $3s^23p^5+e\rightarrow 3s^23p^44pn''l''$ were allowed to interact for all $l''\leqslant 5$, and in a separate calculation, $3s^23p^5+e\rightarrow 3s3p^54dn''l''$ and $3s^23p^5+e\rightarrow 3s^23p^44dn''l''$ were allowed to interact for all $l''\leqslant 5$. Thus limited CI was included in the calculation of the DR rate coefficient for the M-shell $\Delta n=1$ channel in Mo^{25+}. For the $n''=4$ manifold of this ion, it is possible to allow all values of $4l'$ to interact; only a slight difference between the computation with full CI and with limited CI was found. For all manifolds with $n''>4$ each value of the angular quantum number of the excited electron, $4l'$, was computed separately and then summed to find the total contribution to recombination through that manifold.

A comparison of the recombination rate coefficient for the L-shell $\Delta n=1$, M-shell $\Delta n=0$ and $\Delta n=1$ channels for each M-shell ion in the present work is made in Table II.

C. Radiative stabilization channels

1. L-shell $\Delta n=1$ channel

For each recombination channel considered above, there are many competing channels for radiative transitions from

TABLE II. The contribution (in units of 10^{-13} cm^3 sec^{-1}) of the L-shell $\Delta n=1$, M-shell $\Delta n=0$, and M-shell $\Delta n=1$ recombination channels to the total DR rate coefficient as a function of electron temperature.

	Electron temperature (eV)					
Ion charge	500	1000	1500	2000	2500	5000
			L-shell $\Delta n=1$ channel			
24+	35.2	70.9	71.3	63.4	54.8	28.5
25+	38.9	71.3	69.8	61.2	52.6	27.0
30+	208.5	300.2	257.2	234.5	198.1	98.5
31+	235.5	294.2	257.5	214.7	179.1	86.9
			M-shell $\Delta n=0$ channel			
24+	1990.4	755.0	420.9	276.7	199.5	71.6
25+	1398.1	532.2	297.0	195.3	140.8	50.5
30+	574.3	212.1	117.1	76.7	55.1	19.7
31+	267.5	98.6	54.4	35.6	25.6	9.1
			M-shell $\Delta n=1$ channel			
24+	1249.6	574.2	343.4	234.1	172.5	64.8
25+	1196.1	545.2	325.2	221.4	163.0	61.1
30+	417.2	201.0	123.2	85.2	63.3	24.2
31+	209.5	105.7	65.7	45.8	34.2	13.2

TABLE III. Radiative stabilization channels considered in computing the recombination rate coefficient through the L-shell $\Delta n=1$, M-shell $\Delta n=0$, and M-shell $\Delta n=1$ channels in Mo^{24+}, Mo^{25+}, Mo^{30+}, and Mo^{31+}. n_0 indicates the first manifold of the M-shell $\Delta n=0$ channel to include levels which lie in the continuum and is defined for each ion in Table I.

Ar I-like Mo^{24+} $m=2$, $k=6$
Cl I-like Mo^{25+} $m=2$, $k=5$
Mg I-like Mo^{30+} $m=2$, $k=0$
Na I-like Mo^{31+} $m=1$, $k=0$

L-shell $\Delta n=1$

Excitation + capture channels: $[2l^8]3s^m3p^k+e\rightarrow[2l^7]3s^m3p^k3l'n''l''$ (where $n''\leq 15$, $l''\leq 5$)

Stabilization channels:

$[2s2p^6]3s^m3p^k3l'n''l''\rightarrow[2s^22p^5]3s^m3p^k3l'n''l''$
(with possible subsequent autoionization included)

$[2l^7]3s^m3p^k3l'n''l''\rightarrow[2l^7]3s^m3p^{k+1}n''l''$ or $[2l^7]3s^{m+1}3p^kn''l''$
(with possible subsequent autoionization)

$[2l^7]3s^m3p^k3l'n''l''\rightarrow[2l^7]3s^m3p^k3l'nl$ ($n=n''$ and $n=3$)
(with possible subsequent autoionization included where $n=n''$)

$[2l^7]$(core)$3l'n''l''\rightarrow[2l^8]$(core)$n''l''$ (where ''core''=all remaining $3l$ electrons)
(no subsequent autoionization included)

M-shell $\Delta n=0$

Excitation + capture channels: $3s^m3p^k+e\rightarrow3s^{m-1}3p^k3l'n''l''$ (where $n_0\leq n''\leq 19$, $l''\leq 5$)
$3s^m3p^k+e\rightarrow3s^m3p^{k-1}3l'n''l''$ (where $n_0<n''\leq 19$, $l''\leq 5$)

Stabilization channels:

(core)$3l'n''l''\rightarrow$(core)$3ln''l''$ (where ''core''=all remaining $n=3$ electrons)
(with possible subsequent autoionization included)

(core)$3l'n''l''\rightarrow$(core)$3l'nl$ ($n'-4\leq n\leq n''$)
(with possible subsequent autoionization included when $n=n''$)

(core)$3l'n''l''\rightarrow$(core)$3l'nl$ ($n\leq n_0$)
(always stable against autoionization)

M-shell $\Delta n=1$

Excitation + capture channels: $3s^m3p^k+e\rightarrow3s^{m-1}3p^k4l'n''l''$ (where $l'\leq 3$, $n''\leq 12l''\leq 5$)
$3s^m3p^k+e\rightarrow3s^m3p^{k-1}4l'n''l''$ (where $l'\leq 3$, $n''\leq 12l''\leq 5$)

Stabilization channels:

(core)$4l'n''l''\rightarrow$(core)$4ln''l''$ (where ''core''=inactive $n=3$ electrons)
(with subsequent autoionization included)

(core)$4l'n''l''\rightarrow$(core)$4l'nl$ ($n''-1\leq n\leq n''$ and $n=3$ and 4)
(with subsequent autoionization included when $n=n''$)

(core)$4l'n''l''\rightarrow$(core)$3ln''l''$
(possible subsequent autoionization neglected)

the intermediate states, some of which are stabilizing, some of which may subsequently autoionize. In what follows below, only the most important decays will be discussed; *all* radiative decays considered for each recombination channel are listed in Table III. It is indicated in Table III whether the branching ratio for stabilization from the intermediate states of the recombined ion [Eq. (4)] includes subsequent autoionization following radiative transitions between levels in the continuum. In the L-shell $\Delta n=1$ channel the dominant stabilizing mechanism is through an $n=3$ to 2 decay; decays of the form $\overline{2s}$[core]$3l'n''l''\rightarrow\overline{2p}$[core]$3l'n''l''$ and $2l^7$[core]$\overline{3l}n''l''\rightarrow 2l^7$[core]$\overline{3l'}n''l''$, where the overbar indicates a hole in the particular shell, end on states which are unstable against autoionization. In particular, for recombination of Mo^{30+} these are transitions of the form $2s2p^63s^23d4f\rightarrow 2s^22p^53s^23d4f$ and $2s2p^63s^23d4f\rightarrow 2s2p^63s^23p4f$, respectively. Including possible subsequent stabilizing decays from these transitions enhances the rate of recombination in Mo^{30+} through the $n''=3$ manifold by 30% and through the $n''=4$ manifold by 5%. For the $n''=3$ manifold of Mo^{25+} and Mo^{30+} the enhancement of the recombination rate from subsequent stabilization of both types of decays above is found to be less than 5%.

In Fig. 6 the present relativistic, intermediate-coupled calculation for the contributions through the $n''=3$, 4, 5, and 6 manifolds to the total rate coefficient of the L-shell $\Delta n=1$ channel in Mo^{30+} and Mo^{31+} at 2.8 and 3 keV, respectively, are compared to the calculation made by Dube and LaGattuta

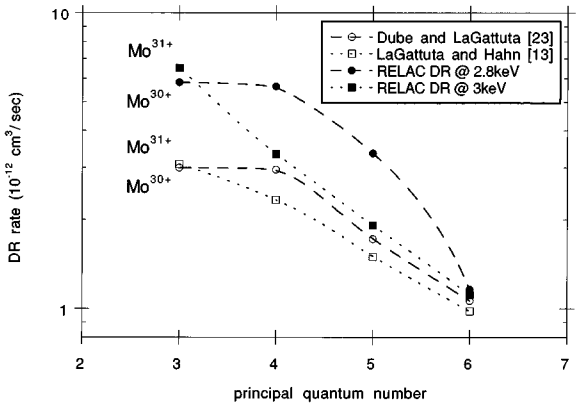

FIG. 6. Comparison between RELAC's Mo^{30+} and Mo^{31+} L-shell $\Delta n=1$ channel DR rates (solid icons) and previously published nonrelativistic values for Mo^{30+} from Ref. [23] (open squares) and for Mo^{31+} from Ref. [13] (open circles). The lines drawn through the data for each ion merely aid the eye and have no mathematical meaning.

[23] and LaGattuta and Hahn [13]. The contribution for each manifold computed in the present work is significantly larger than the nonrelativistic results of Refs. [23,13]. This is due, in part, to the detailed calculation of the ionic level structure, and primarily, to the larger radiative width for each doubly excited manifold that results from the intermediate-coupling calculation of radiative transition rates. Many transitions which are LS forbidden in Refs. [23,13] have nonzero probabilities in the present work.

2. M-shell $\Delta n=0$ channel

Radiative decays of the form $2l^8[\text{core}]3l'n''l''\rightarrow 2l^8[\text{core}]3ln''l''$, where ''core'' represents all inactive electrons of the $n=3$ shell, are the dominant stabilizing mechanism for the M-shell $\Delta n=0$ channel. In Mo^{25+} this would be a decay of the form $3s3p^5 3d8g\rightarrow 3s3p^6 8g$. The final state of these decays may be unstable against autoionization; in this case, subsequent autoionization and possible stabilization is taken into account in computing the total branching ratio for stabilization in Eq. (4). Radiative decays involving the outer electron to states that are always stable against subsequent autoionization $[\text{core}]3l'n''l''\rightarrow[\text{core}]3l'nl(n\leqslant n_0)$ are also allowed to take place. Based on the observed dominance of the (usually stabilizing) $3l'\rightarrow 3l$ transitions, and the large width for $n''l''\rightarrow nl(n\leqslant n_0)$ stabilizing, radiative transitions we estimate neglecting subsequent autoionization from the $n''l''\rightarrow nl(n>n_0)$ decays overestimates the contribution of the highest-energy manifolds in this channel to the total DR rate by no more than 10%. The contribution of the manifolds with $n''\geqslant n_0$ is from 80% to 90% of the total DR rate through the M-shell $\Delta n=0$ channel. A significant enhancement of the DR rate through the M-shell $\Delta n=0$ channel results from carrying out the present calculation in intermediate coupling; many LS-forbidden stabilizing channels are enabled in an intermediate-coupled calculation, thus increasing the total width for radiative stabilization. For example, in Mo^{31+} at 3 keV, the present result is a factor of 2.2 larger than the contribution of all orbitals with angular quantum numbers $\leqslant 5$ in Ref. [13] (see Table IV of Ref. [13]).

D. Summary

The total recombination rate coefficient calculated from Eq. (2) for the ground state of Mo^{33+} to Mo^{30+}, Mo^{25+}, and Mo^{24+} is listed in Table IV and is plotted versus temperature in Fig. 7. To ensure that the calculated contribution from each channel to the total DR rate for each ion is converged, an n^{-3} scaling has been used to estimate the contribution to the total rate of all manifolds above those listed in Table I. The total DR rate may be overestimated by as much as 15% at temperatures above 2 keV due to the neglect of autoionization from the intermediate states of the L- and M-shell $\Delta n=1$ channels to highly excited states of the initial ion. Below 2 keV, the dominant channel is the M-shell $\Delta n=0$ channel; the DR rates below 2 keV are estimated to be accurate to $\pm 10\%$. A 10% underestimate of the total rates is possible due to the neglect of electron capture into orbitals with angular quantum numbers $l''\geqslant 6$.

III. EXCITATION-AUTOIONIZATION

A. Calculation of excitation autoionization rate coefficients

Ab initio calculations of the rate of excitation by electron impact followed by autoionization have been performed for molybdenum charge states Mo^{23+}, Mo^{24+}, and Mo^{29+} to Mo^{32+}. As in the case of DR, only the rate of excitation autoionization from the ground state of each ion has been considered. The contribution to the total EA rate from metastable energy levels near the ground level is an area of ongoing research. The agreement obtained between the experimental profiles of the Mo^{33+} and Mo^{31+} ions in Fig. 1 and the predicted profiles made using the data in the present work allows us to conclude that the data here are adequate for modeling of low-density (tokamak) plasmas.

The EA rate from level i of ion $q+$ is given by

$$S_i^{\text{EA}}(T_e)=\sum_j\left[Q_{ij}(T_e)\,\frac{\sum_f A^a_{j,f}}{\sum_i A^r_{j,i}+\sum_f A^a_{j,f}}\right], \qquad (9)$$

where $Q_{ij}(T_e)$ is the electron-impact excitation rate in $\text{cm}^3\,\text{sec}^{-1}$ from the level i of ion $q+$ to an intermediate state j of ion $q+$ above the ionization limit, and f is an energy level in ion $(q+1)+$. Efficient calculation of the EA rate for these molybdenum ions is possible as a result of the factorization-interpolation method of Bar-Shalom, Klapisch, and Oreg [37] for impact excitations. The electron-impact excitation rates are calculated in the distorted wave approximation by CROSS [37] using RELAC's relativistic wave functions.

B. Excitation channels

Computation of the EA rate coefficient is simpler than computation of the DR rate coefficient because only levels above the continuum reachable by a single excitation from the ground state of ion $q+$ need to be considered. Table V lists the inner-shell excitation channels, the final states for autoionization, and the radiative stabilization channels in the

TABLE IV. The dielectronic recombination rate coefficient for Mo^{24+}, Mo^{25+}, Mo^{30+}, Mo^{31+}, Mo^{32+}, and Mo^{33+} as a function of electron temperature in units of 10^{-12} $cm^3\,sec^{-1}$. Numbers in parentheses represent powers of 10, that is, $X(-Y)$ means $X\times10^{-Y}$.

T_e (keV)	Mo^{24+}	Mo^{25+}	Mo^{30+}	Mo^{31+}	Mo^{32+}	Mo^{33+}
0.050	2965.4	2024.8	1317.2	548.3	1.97(−4)	41.9
0.100	1752.2	1305.1	645.0	284.7	9.75(−2)	25.0
0.150	1211.9	927.1	409.0	185.4	0.9	19.3
0.200	910.7	707.0	295.6	138.3	2.6	19.1
0.300	590.5	466.2	191.5	97.4	7.4	24.4
0.400	425.8	339.8	145.3	80.5	12.3	30.1
0.500	327.5	263.3	120.0	71.2	16.7	34.1
0.600	263.1	212.7	104.0	65.1	20.2	36.5
0.800	184.9	150.8	84.1	56.4	24.5	38.2
1.000	140.0	114.9	71.3	49.8	26.3	37.4
1.200	111.2	91.6	62.0	44.4	26.4	35.4
1.400	91.3	75.5	54.7	39.8	25.7	33.1
1.600	76.9	63.7	48.7	35.9	24.6	30.8
1.800	65.9	54.8	43.8	32.5	23.3	28.5
2.000	57.4	47.8	39.6	29.6	22.0	26.4
2.200	50.6	42.2	36.1	27.1	20.7	24.5
2.400	45.1	37.6	33.0	24.9	19.5	22.8
2.600	40.5	33.8	30.4	22.3	18.3	21.2
2.800	36.6	30.6	28.1	21.3	17.2	19.8
3.000	33.4	27.9	26.0	19.7	16.2	18.5
3.200	30.6	25.6	24.2	18.4	15.3	17.4
3.400	28.1	23.6	22.6	17.2	14.5	16.3
3.600	26.0	21.8	21.1	16.1	13.7	15.4
3.800	24.1	20.3	19.9	15.2	13.0	14.5
4.000	22.5	18.9	18.7	14.2	12.3	13.7
4.200	21.0	17.7	17.6	13.5	11.7	13.0
4.400	19.7	16.6	16.7	12.8	11.1	12.3
4.600	18.5	15.6	15.8	12.1	10.6	11.7
4.800	17.4	14.7	15.0	11.5	10.1	11.1
5.000	16.5	13.9	14.2	10.9	9.7	10.6

EA calculation for each ion. For every ion considered, the dominant type of excitation producing an autoionizing state is of the form

$$2l^8[3s^m3p^k3d^r]+e\rightarrow2l^7[3s^m3p^k3d^r]n'l'+e, \quad (10)$$

where $l=s$ or p; for example, in aluminumlike Mo^{29+} the dominant EA channel proceeds through $2s^22p^63s^23p\rightarrow2s^22p^53s^23pn'd$. The calculation of the EA rate coefficient through the above L-shell excited manifolds has been truncated for each ion at some value of n' by requiring that the EA rate through $2l^8[\text{core}]\rightarrow2l^7[\text{core}]n'l'$ be less than 0.5% of the sum of the EA rates through all manifolds $2l^8[\text{core}]\rightarrow2l^7[\text{core}]n''l''$ with $n''<n'$. Consideration of angular momentum values $l'>4$ is unnecessary since excitations of a $2s$ and $2p$ electron to states with $l'>4$ are dipole forbidden and will be very small. Including subsequent autoionization from radiative transitions between continuum states in the branching ratio toward autoionization [Eq. (9)] increases the contribution of an L-shell excited manifold to the total EA rate by less than 5%. This is due to the dominance of optically allowed $3l'\rightarrow2l$ stabilizing transitions in the branching ratio in Eq. (9).

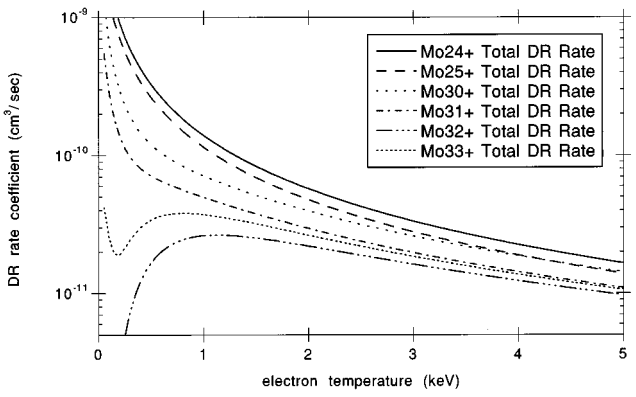

FIG. 7. The total DR rate coefficients for L- and M-shell molybdenum ions between 50 and 5000 eV.

In Mo^{23+} and Mo^{24+}, the contributions to the total EA rate from M-shell excitations of the form $3l\rightarrow n'l'$ with $l=s$ or p and $n'\leqslant15$, $l'\leqslant5$ have been computed; for example, in K I-like Mo^{23+}, excitations of the form $3s^23p^63d\rightarrow3s3p^63dn'l'$ and $3s^23p^63d\rightarrow3s^23p^53dn'l'$ have been considered. The M-shell excitations and stabilization channels for these ions are shown in Table V. For

TABLE V. Configurations used in computing the EA rate coefficient for Mo^{23+}, Mo^{24+}, Mo^{29+}, Mo^{30+}, Mo^{31+}, and Mo^{32+}. Also shown are final states for autoionization and radiative decay channels. Indication has been made where radiative decays may not be stable against subsequent autoionization.

Excitation channels: L shell: $[2l^7]3s^m3p^k3d^rn''l''$ (where $3\leqslant n''\leqslant 7$, $l''\leqslant 4$)
M shell: $[2l^8]3s^{m-1}3p^k3d^rn''l''$ (where $6\leqslant n''\leqslant 15$, $l''\leqslant 5$)
$[2l^8]3s^m3p^{k-1}3d^rn''l''$ (where $8\leqslant n''\leqslant 15$, $l''\leqslant 5$)

K I-like Mo^{23+} $m=2$, $k=6$, $r=1$

Final autoionization states: $3s^23p^6$, $3s^23p^53d$, $3s3p^63d$, $3s^23p^54l$ ($l\leqslant 3$)

Ar I-like Mo^{24+} $m=2$, $k=6$, $r=0$

Final autoionization states: $3s^23p^5$, $3s^23p^43d$, $3s3p^6$, $3s^23p^44l$ ($l\leqslant 3$)

Stabilization channels:

L-shell:

$[2s2p^6]3s^m3p^k3d^rn''l''\rightarrow[2s^22p^5]3s^m3p^k3d^rn''l''$
(subsequent autoionization neglected)

$[2l^7]3s^m3p^k3d^rn''l''\rightarrow[2l^7]3s^m3p^k3d^rn'l'$ ($n''-3\leqslant n'\leqslant n''$ and $n'=3$)
(subsequent autoionization neglected)

$[2l^7]$(core)$3l'n''l''\rightarrow[2l^8]$(core)$n''l''$ (where ''core''=all remaining $3l$ electrons)
(no subsequent autoionization possible)

$[2l^7]3s^m3p^k3d^rn''l''\rightarrow[2l^8]3s^m3p^k3d^r$
(no subsequent autoionization possible)

M-shell:

$[2l^8]3s^{m-1}3p^k3d^rn''l''\rightarrow[2l^8]3s^m3p^{k-1}3d^rn''l''$
(subsequent autoionization neglected)

$[2l^8]3s^m3p^{k-1}3d^rn''l''\rightarrow[2l^8]3s^m3p^kn''l''$
(no subsequent autoionization)

$[2l^8]3s^{m-1}3p^k3d^rn''l''\rightarrow[2l^8]3s^{m-1}3p^k3d^rn'l'$ ($n''-3\leqslant n'\leqslant n''$ and $n'=3$)
(possible subsequent autoionization neglected,
no subsequent autoionization when $n'=3$)

$[2l^8]3s^m3p^{k-1}3d^rn''l''\rightarrow[2l^8]3s^m3p^{k-1}3d^rn'l'$ ($n''-3\leqslant n'\leqslant n''$ and $n'=3$)
(possible subsequent autoionization neglected,
no subsequent autoionization when $n'=3$)

Excitation channels: $[2l^7]3s^m3p^kn''l''$ (where $3\leqslant n''\leqslant 8$, $l''\leqslant 4$)

Al I-like Mo^{29+} $m=2$, $k=1$

Final autoionization states: $3s3l$ ($l\leqslant 2$)

Mg I-like Mo^{30+} $m=2$, $k=0$

Final autoionizatioin states: $3l$ ($l\leqslant 2$)

Na I-like Mo^{31+} $m=1$, $k=0$

Final autoionization states: $2s^22p^6$

Stabilization channels:

$[2s2p^6]3s^m3p^kn''l''\rightarrow[2s^22p^5]3s^m3p^kn''l''$
(subsequent autoionization neglected)

$[2l^7]3s^m3p^kn''l''\rightarrow[2l^7]3s^m3p^kn'l'$ ($n''-3\leqslant n'\leqslant n''$ and $n'=3$)
(subsequent autoionization neglected)

$[2l^7]$(core)$3l'n''l''\rightarrow[2l^8]$(core)$n''l''$ (where ''core''=all remaining $3l$ electrons)
(no subsequent autoionization possible)

$[2l^7]3s^m3p^kn''l''\rightarrow[2l^8]3s^m3p^k$
(no subsequent autoionization possible)

Excitation channels: $[2s^2(2p_{1/2})(2p_{3/2})^4]n''l''$ (where $12\leqslant n''\leqslant 15$, $l''\leqslant 3$)
$[2s(2p)^6]n''l''$ (where $7\leqslant n''\leqslant 10$, $l''\leqslant 3$)

Ne I-like Mo^{32+}

Final autoionization states: $2s^22p^5$

Stabilization channels:

$[2s2p^6]n''l''\rightarrow[2s^22p^5]n''l''$
(no subsequent autoionization possible)

$[2l^7]n''l''\rightarrow[2l^7]n'l'$ ($3\leqslant n'\leqslant n''$)
(subsequent autoionization neglected)

$[2l^7]n''l''\rightarrow[2l^8]$
(no subsequent autoionization possible)

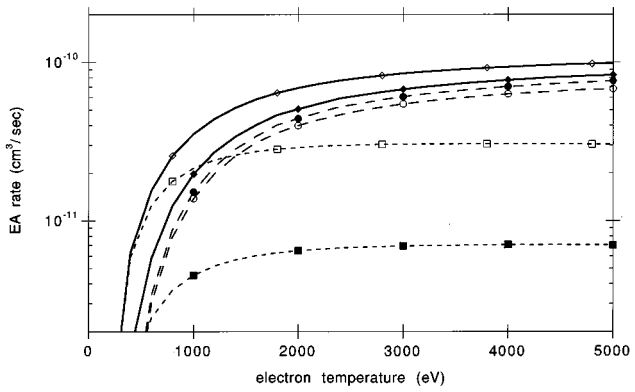

FIG. 8. The Mo^{23+} (open icons) and Mo^{24+} (filled icons) total EA rate coefficients (diamonds, solid lines) from 50 to 5000 eV and the L- (circles, long dashes) and M- (squares, short dashes) shell excitation contributions to the total EA rate coefficients.

Mo^{23+}, excitations from orbitals with both $l=s$ and p can contribute to the EA rate. For Mo^{24+} (and all charge states to aluminumlike Mo^{29+}) only excitations from orbitals with $l=s$ can contribute to the EA rate; the $3s^2 3p^{k-1} n'l'$ excited states converge to the ground state, $3s^2 3p^{k-1}$, of the next ion and cannot autoionize. The small overlap of the $3s$ and $3p$ orbitals with excited orbitals having $l'>4$ means states with large angular quantum numbers do not need to be considered in computing the M-shell excitations' contribution to the EA rate coefficients for the Mo^{23+} and Mo^{24+} ions. The total EA rate for Mo^{23+} (open diamonds) and Mo^{24+} (filled diamonds), and the L- and M-shell contributions to the EA rate for each ion are shown in Fig. 8. The L-shell channel for EA in all ions presently considered is the dominant contribution to the total rate; as seen in Fig. 8, the M-shell contribution need only be considered for Mo^{23+}.

The contribution to the total Mo^{29+} EA rate from the $2l^8[\text{core}] \rightarrow 2l^7[\text{core}]n'l'$ $n'=3$ and 4 manifolds has been computed simultaneously, thus allowing CI effects on level energies and transition probabilities between levels of different manifolds. The contribution from all $2l^8[\text{core}] \rightarrow 2l^7[\text{core}]n'l'$ excited aluminumlike levels with $n'=5$ and 6 (and, in like manner, $n'=7$ and 8) have been computed allowing these respective manifolds to mix. States such as $2s^2 2p^5 3s^2 3d^2$ and $2s^2 2p^5 3s 3p^2 3d$, which cannot be formed by a single excitation from the ground state, are included in the calculations above to account for possible mixing effects. The presence of these doubly excited states is found to enhance (slightly) the autoionization transition probabilities for the $2l^8[\text{core}] \rightarrow 2l^7[\text{core}]n'l'$ $n'=3$ and 4 manifolds, higher manifolds are unaffected. As in the case of Mo^{24+}, the $3s \rightarrow n'l'$ M-shell excitations in Mo^{29+} can autoionize to the ground state of the next ion; this channel has been neglected in the calculation of the total EA rate coefficient for Mo^{29+} based on the behavior shown in Fig. 8.

For Mo^{30+}, the contribution to the total EA rate from all $2l^8[\text{core}] \rightarrow 2l^7[\text{core}]n'l'$ manifolds with $n' \leqslant 6$ has been computed with full CI between all excited states; the set of doubly and triply excited states of the form $\overline{2l}3l3l'3l''$ (where $\overline{2l}$ indicates a $2l$-shell hole) for all possible values of l, l', and l'' are also included in the calculation. The contributions from the $n'=7$ and 8 manifolds to the total EA rate coefficient in Mo^{30+} were computed separately. For Mo^{31+}, the contribution to the total EA coefficient from all $2l^8[\text{core}] \rightarrow 2l^7[\text{core}]n'l'$ manifolds with $n' \leqslant 8$ has been computed allowing the full spectrum of CI effects between the levels of the different manifolds; the full set of doubly excited states of the form $\overline{2l}3l'3l''$ are also included in the calculation to account for mixing effects. CI enhances some of the radiative and autoionization transition rates for these ions. However, the global effect of CI on the EA rate through a particular L-shell excited manifold is observed to be negligible. There is no M-shell contribution to the Mo^{30+} or Mo^{31+} ground-state EA rate; no complex of levels formed by direct excitation of a $3s$ electron can autoionize to the ground state of the next ion (these states only converge to the ground state of the next ion).

The absence of any M-shell electrons in the Mo^{32+} ion means the ionization potential of this ion is much larger than those of the preceding charge states (the ionization potential of Mo^{31+} is $\sim$1.8 keV, the ionization potential of Mo^{32+} is greater than 4.2 keV). There are no strongly coupled $n=2$ to $n=3,4,\ldots$ excitation channels leading to autoionizing states in Ne I-like Mo^{32+} as in the preceding charge states: the first $2s$ excitation to lie above the ionization potential of Mo^{32+} is $2s2p^6 7s$. Additional EA cross section in this ion arises from the wide energy splitting [38] of the $2p_j^5 nl$ excited levels of Mo^{32+} based on the j value of the $2p$ hole (either $j=\frac{3}{2}$ or $j=\frac{1}{2}$); the first $2p^5 nl$ level to lie above the ground state of Mo^{33+} ($2p^5 J=\frac{3}{2}$) is from a configuration with $n=12$. The EA rate for Mo^{32+} through excitations of the form $2p_{1/2} \rightarrow n'l'$ for $12 \leqslant n' \leqslant 15$, $l' \leqslant 4$ and $2s \rightarrow n'l'$ for $7 \leqslant n' \leqslant 10$, $l' \leqslant 4$ has been computed. The highly excited nature (weak collisional coupling) of the L-shell EA channels in Mo^{32+} means the resulting EA rate coefficient is small compared to the rate coefficients for the M-shell ions.

The EA rate coefficient for Mo^{23+}, Mo^{24+}, and Mo^{29+} to Mo^{32+} are listed in Table VI. Due to the neglect of subsequent autoionization from the final states of radiative transitions between levels in the continuum, the EA rate coefficients in this section may be underestimated by as much 10%. A plot of the EA rate coefficients as a function of temperature is shown in Fig. 9.

IV. GENERATED RATE COEFFICIENTS

A. Fits for the DR and EA rate coefficients

The large differences between the rates computed for DR and EA in the present work and less accurate rates often used in plasma modeling codes suggest that a consistent treatment for all ions from Mo^{23+} to Mo^{33+} is required. The *ab initio* calculations of the two preceding sections allow us to make estimates of the DR and EA rates for the charge states which exist between the ions treated above. The method used to generate the total ground-state DR rate coefficients for Mo^{26+} to Mo^{29+} and the ground-state EA rate coefficients for Mo^{25+} to Mo^{28+} follows.

(1) Simple expressions which reflect the behavior of the DR coefficient for each channel, and the EA coefficient as a whole are fit to the calculated rates for each ion from Secs. II and III *at a fixed, characteristic temperature*.

(2) Using the resulting charge-dependent forms, the DR coefficient of each channel and the total EA coefficient for

TABLE VI. The excitation-autoionization rate coefficients (in units of 10^{-13} cm^3 sec^{-1}) for Mo^{23+}, Mo^{24+}, Mo^{29+}, Mo^{30+}, Mo^{31+}, and Mo^{32+} as a function of electron temperature. Numbers in parentheses represent powers of 10, that is, $X(-Y)$ means $X\times10^{-Y}$.

T_e (keV)	Mo^{23+}	Mo^{24+}	Mo^{29+}	Mo^{30+}	Mo^{31+}	Mo^{32+}
0.200	4.7	0.6	0.01	0.01	0.01	5.1(−8)
0.400	63.0	14.9	4.9	4.4	3.2	1.7(−3)
0.600	156.3	58.4	35.1	30.8	23.1	0.05
0.800	257.2	124.1	92.6	80.0	61.6	0.3
1.000	353.2	197.8	162.6	139.5	107.9	0.7
1.200	440.3	271.6	234.5	199.7	155.6	1.3
1.400	516.2	340.3	302.4	256.6	201.0	2.0
1.600	585.9	402.7	364.0	307.9	242.4	2.7
1.800	640.6	465.8	418.8	354.2	279.7	3.5
2.000	689.4	505.8	467.1	393.9	311.7	4.2
2.200	730.0	548.6	506.8	428.9	340.8	4.9
2.400	766.2	593.0	543.9	459.4	370.8	5.6
2.600	798.0	620.0	576.8	486.3	387.2	6.2
2.800	826.0	649.4	605.3	510.0	406.4	6.8
3.000	851.2	675.7	631.0	530.6	425.3	7.3
3.200	872.2	699.5	654.6	550.0	440.4	7.7
3.400	889.9	720.3	673.3	565.0	451.5	8.2
3.600	906.6	739.2	691.0	578.7	463.3	8.5
3.800	921.7	756.4	706.7	591.3	473.7	8.9
4.000	935.1	772.0	720.8	602.7	482.9	9.2
4.200	947.2	785.8	733.6	613.0	491.3	9.5
4.400	958.2	799.0	745.6	622.4	498.9	9.8
4.600	969.0	810.1	756.1	630.4	505.4	10.1
4.800	976.8	820.9	765.1	638.1	511.3	10.3
5.000	984.8	831.7	773.7	644.8	516.7	10.5

the remaining charge states is then generated at the characteristic temperature.

(3) Using the well-known temperature dependence of DR rate coefficients, and a standard form for an impact excitation rate coefficient, one and two parameter fits to the calculated data in Secs. II and III are made; formulas with the above temperature dependencies are forced to pass through the rates generated at the characteristic temperature for the remaining charge states.

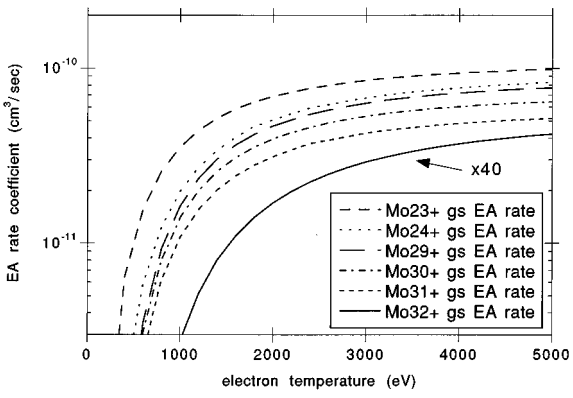

FIG. 9. Calculated EA rate coefficients for L- and M-shell molybdenum ions between 50 and 5000 eV. The rate for Mo^{32+} has been multiplied by a factor of 40 to be visible on the same axis.

B. DR

For the L- and M-shell $\Delta n=1$ DR channels, the form

$$f_{\text{channel}}(q,T_{\text{fixed}})\approx m_1 q^4 \exp(-m_2 q^2)\,\alpha^{\text{DR}}_{\text{channel}}(T_{\text{fixed}})$$

and for the M-shell $\Delta n=0$ DR channel, the form

$$f_{\text{channel}}(q,T_{\text{fixed}})\approx m_1 q\ \exp(-m_2 q)\,\alpha^{\text{DR}}_{\text{channel}}(T_{\text{fixed}})$$

has been least-squares fit to the explicitly calculated DR rate coefficient for Mo^{32+} to Mo^{30+} and Mo^{25+} and Mo^{24+} at a fixed temperature. In the two expressions above, $q+$ is the charge on each ion and m_1 and m_2 are determined by the fit. The function $\alpha(T_{\text{fixed}})$ represents the temperature-dependent part of the DR rate coefficient for each channel, and is discussed below. These forms are based on the well-known q-dependent behavior of transition energies and dipole allowed $\Delta n\neq0$ and $\Delta n=0$ transition rates [39], respectively. The DR rates chosen for the expressions above were taken at $T_e=3$ keV for the L-shell $\Delta n=1$ channel, and at 1.5 and 2.0 keV for the M-shell $\Delta n=0$ channel and M-shell $\Delta n=1$ channels, respectively. The fit for each channel is then used to interpolate the DR rate coefficient *at the characteristic temperature* of the $3s^2 3p^k$ ($k=2$–4) isosequences.

The form used by Teng *et al.* in Ref. [21] (see references by the same authors therein) has been used to fit the temperature dependence of the *ab initio* calculations of the L- and

TABLE VII. The coefficients of the functional form in Eq. (11) for the L- and M-shell contributions to the total dielectronic recombination rate coefficient for molybdenum ions Mo^{33+} to Mo^{24+}.

Ion charge	A_1	B_1	A_2	B_2
		L-shell $\Delta n=0$		
33+	0.031 223	0.058 696		
		L-shell $\Delta n=1$		
24+	0.934 30	1.827 6		
25+	0.862 66	1.737 2		
26+	1.083 9	1.737 2		
27+	1.362 0	1.737 2		
28+	1.711 3	1.737 2		
29+	2.150 3	1.737 2		
30+	1.972 8	2.258 2	1.3172	1.1468
31+	0.960 17	0.960 33	1.8385	2.0143
32+	1.093 6	1.180 0	2.2586	2.3328
33+	1.149 7	0.916 36	2.2296	2.0609
		M-shell $\Delta n=0$		
24+	1.516 8	0.049 009		
25+	1.102 6	0.057 812		
26+	0.923 12	0.057 812		
27+	0.771 73	0.057 812		
28+	0.644 29	0.057 812		
29+	0.559 58	0.042 690		
30+	0.435 93	0.032 123		
31+	0.206 18	0.034 293		
		M-shell $\Delta n=1$		
24+	0.453 20	0.067 254	1.122 0	0.377 24
25+	0.448 74	0.064 965	1.036 9	0.374 94
26+	0.403 13	0.064 965	0.931 49	0.374 94
27+	0.360 02	0.064 965	0.831 88	0.374 94
28+	0.319 76	0.064 965	0.738 85	0.374 94
29+	0.282 56	0.064 965	0.652 88	0.374 94
30+	0.159 22	0.036 255	0.430 18	0.488 40
31+	0.072 275	0.055 676	0.252 09	0.509 63

M-shell channel contributions to the total DR rate coefficient for Mo^{33+} to Mo^{30+} and Mo^{25+} and Mo^{24+}:

$$\alpha^{\mathrm{DR}}(T_e)=\frac{4.8\times10^{-11}}{T_e^{3/2}}\sum_{i=1}^{m}A_i\exp\left(-\frac{B_i}{T_e}\right), \qquad (11)$$

where T_e is the electron temperature in keV, and the coefficients A_i and B_i are listed in Table VII. The fit of Eq. (11) to the *ab initio* rate coefficients of Sec. II is accomplished using the Levenberg-Marquardt method [40]. Since the temperature dependence of the DR process is well known, Eq. (11) has been forced to pass through the generated rate coefficients for each channel in Mo^{29+} to Mo^{26+}. The resulting values of A_i and B_i are also listed in Table VII.

Equation (11) fits the calculated data for the L-shell $\Delta n=1$ excitation channel in the lower charge states, Mo^{24+} to Mo^{25+}, with a single term, i.e., $m=1$. This reflects the dominant (relative) contribution of the $2p\rightarrow3d$ excitations to the total rate of recombination through this channel. The higher charge states, Mo^{30+} to Mo^{32+}, are fit by a two term sum, i.e., $m=2$, reflecting the larger (relative) contribution from the $2s\rightarrow3p$ and $2s\rightarrow3s$ excitations to the rate of recombination in these ions. The values generated by Eq. (11) fit the calculated L-shell $\Delta n=1$ rates to better than 1% accuracy at temperatures above 1.5 keV and to better than 3% for temperatures below 1.5 keV. Equation (11) achieves very accurate fits to the data of the M-shell $\Delta n=0$ channel with only a single term. This is true despite the presence of two excitation channels ($3s\rightarrow3l$ and $3p\rightarrow3d$) in the lower charge states. The values generated by Eq. (11) fit the calculated rates in this channel to better than 1% accuracy at all temperatures. For the M-shell $\Delta n=1$ channel, Eq. (11) requires a sum with two terms in every case, i.e., $m=2$, to fit the data. The values generated by Eq. (11) fit the calculated rates in the M-shell $\Delta n=1$ channel to better than 1% accuracy at all temperatures.

C. EA

The same procedure described above for DR has been used for EA; the calculated *total* EA rates for Mo^{23+}, Mo^{24+}, and Mo^{29+} to Mo^{31+} at 2 keV have been least-squares fit by the form

$$f_{\mathrm{EA}}(q,T_{\mathrm{fixed}})\approx\exp(-m_1q^2)S^{\mathrm{EA}}(T_{\mathrm{fixed}}),$$

where $q+$ is the ionic charge, m_1 is given by the fit, and the calculated rate coefficients at T_e have been used for $S^{\mathrm{EA}}(T_{\mathrm{fixed}})$. No attempt has been made to fit separately the L- and M-shell contributions to the total EA rate for Mo^{23+} and Mo^{24+}. The EA rates for Mo^{25+}, Mo^{26+}, Mo^{27+}, and Mo^{28+} at $T_e=2$ keV have been interpolated using the above fit to the calculated data.

For all charge states considered in the present work (except Mo^{32+}), the branching ratio towards autoionization from $n=2$ inner-shell excited manifolds is quite large, and experiences no discontinuities due to the sudden closing of autoionizing channels in adjacent charge states. The form of a sum of collisional-excitation rate coefficients has been fit to the *ab initio* EA rates for Mo^{23+}, Mo^{24+}, and Mo^{29+} to Mo^{32+} by using the Levenberg-Marquardt method:

$$S^{\mathrm{EA}}(T_e)=\frac{4.5\times10^{-11}}{T_e^{1/2}}\left[\sum_{i=1}^{2}C_i\exp\left(\frac{-D_i}{T_e}\right)\right], \qquad (12)$$

where T_e is the electron temperature in keV and the values of C_i and D_i are listed in Table VIII. The total EA rate for the remaining charge states, Mo^{25+} to Mo^{28+}, has been found by requiring Eq. (12) to pass through the points generated at 2 keV. The form chosen for Eq. (12) fits the calculated EA rate coefficients for all the charge states to better than 3% at temperatures above 1.5 keV. For Mo^{32+} to Mo^{29+} the fit rates match the calculated rates to 3% accuracy at the lowest temperatures. For Mo^{24+} and Mo^{23+} the fit rates match the calculated rates to better than 5% below 1 keV; this larger discrepancy results from the presence of the M-shell EA channel in the calculation of the total rate coefficient for these two ions.

V. DISCUSSION OF RESULTS

The extensive calculations of the present work have been applied to modeling observations of the spatial distribution

TABLE VIII. The coefficients of the functional form in Eq. (12) for the excitation-autoionization rates for molybdenum ions Mo^{23+} to Mo^{32+}.

Ion charge	C_1	D_1	C_2	D_2
23+	6.5655	3.3623	1.7631	1.1877
24+	6.4849	3.2091	0.69059	1.4177
25+	3.4271	4.7194	4.4732	2.5549
26+	3.3729	4.7194	4.4024	2.5549
27+	3.3196	4.7195	4.3328	2.5549
28+	3.2671	4.7194	4.2643	2.5549
29+	3.2154	4.7195	4.1969	2.5549
30+	2.551	4.9597	3.6763	2.5583
31+	2.0563	4.8934	2.9518	2.5917
32+	0.1183	4.3225		

of the Mo^{33+} to Mo^{23+} ions in a high-temperature, low-density plasma. The *ab initio* calculations of the DR and EA rate coefficients described in the present work are responsible for a large reduction in the predicted equilibrium temperatures for these ions from the equilibrium temperatures in the plasma predicted by less accurate models. The atomic data package (ADPAK) [6] in the widely used plasma modeling code MIST [8] has been found inadequate to predict the observed molybdenum charge state distributions in a tokamak plasma; incorporation of the atomic data of the present work in the MIST code removes the discrepancies between the MIST model and observations. The DR rates for the ions in the present paper are often larger than the same rates in ADPAK. A greater enhancement of the ionization rates in ADPAK for the ions in the present paper is achieved by the addition of the EA process to the direct ionization rate. The resulting *net* enhancement of ionization rates means that the present ions appear at a lower temperature in the plasma than previously predicted. The dramatic difference seen between the computed profiles in Fig. 1 can be understood to result from an improvement in the quality of the underlying atomic data. A full discussion of the observations and the plasma models mentioned here can be found in a paper by Rice *et al.* [7].

ACKNOWLEDGMENT

The present work was performed under the auspices of the U.S Department of Energy by the Lawrence Livermore National Laboratories under Contract No. W-7405-ENG-48.

[1] I. H. Hutchinson *et al.*, Phys. Plasmas **1**, 1511 (1994).
[2] E. Hinnov *et al.*, Nucl. Fusion **18**, 1305 (1978).
[3] R. C. Isler, Nucl. Fusion **24**, 1599 (1984).
[4] C. DeMichelis and M. Mattioli, Rep. Prog. Phys. **47**, 1233 (1984).
[5] F. Wagner and K. Lackner, in *Physics of Plasmas—Wall Interactions in Controlled Fusion*, edited by D. Post and R. Behrisch (Plenum, New York, 1984).
[6] D. Post, R. Jensen, C. B. Tarter, W. Grasberger, and W. Lockke, At. Data Nucl. Data Tables **20**, 397 (1977).
[7] J. Rice *et al.*, J. Phys. B **29**, 2191 (1996).
[8] R. Hulse, Nucl. Technology/Fusion **3**, 259 (1983).
[9] A. Burgess, Astrophys. J. **139**, 776 (1964); **141**, 1588 (1965).
[10] M. J. Seaton and P. J. Storey, in *Atomic Processes and Applications*, edited by P. G. Burke and B. L. Moiseiwitsch (North-Holland, Amsterdam, 1976), p. 133.
[11] A. Merts, R. Cowan, and N. Magee, Los Alamos Scientific Laboratory Report No. LA-6220-MS, 1976 (unpublished).
[12] K. LaGattuta and Y. Hahn, Phys. Rev. A **24**, 785 (1981).
[13] K. LaGattuta and Y. Hahn, Phys. Rev. A **30**, 316 (1984).
[14] M. Chen, Phys. Rev. A **34**, 1073 (1986).
[15] S. Dalhed, J. Nilsen, and P. Hagelstein, Phys. Rev. A **33**, 264 (1986).
[16] L. Roszman, Phys. Rev. A **20**, 673 (1979).
[17] Y. Hahn, J. Gau, R. Luddy, and J. Retter, J. Quant. Spectrosc. Radiat. Transfer **23**, 65 (1980).
[18] M. Chen, Phys. Rev. A **38**, 2332 (1988).
[19] L. Roszman, Phys. Rev. A **35**, 2138 (1987).
[20] M. Chen, Phys. Rev. A **34**, 1079 (1986).
[21] H. Teng, Z. Xu, W. Zhang, and B. Shen, Phys. Scr. **50**, 55 (1944); H. Teng, Z. Xu, B. Shen, and W. Zhang, *ibid*. **49**, 696 (1994).
[22] M. Dube, R. Rasoanaivo, and Y. Hahn, J. Quant. Spectrosc. Radiat. Transfer **33**, 13 (1985).
[23] M. Dube and K. LaGattuta, J. Quant. Spectrosc. Radiat. Transfer **38**, 311 (1987).
[24] Y. Hahn, J. Quant. Spectrosc. Radiat. Transfer **49**, 81 (1993); **51**, 663 (1994).
[25] D. H. Crandall, R. Phaneuf, D. Gregory, A. Howald, D. Mueller, T. Morgan, G. Dunn, D. Griffin, and R. Henry, Phys. Rev. A **34**, 1757 (1986).
[26] D. C. Griffin, M. Pindzola, and C. Bottcher, Phys. Rev. A **36**, 3642 (1987).
[27] K. J. Reed, M. Chen, and D. Moores, Phys. Rev. A **44**, 4336 (1991).
[28] K. LaGattuta and Y. Hahn, Phys. Rev. A **24**, 2273 (1981).
[29] A. L. Osterheld, R. Walling, B. Young, W. Goldstein, G. Shimkaveg, B. MacGowan, L. DaSilva, R. London, D. Matthews, and R. Stewart, J. Quant. Spectrosc. Radiat. Transfer **51**, 263 (1994).
[30] A. L. Osterheld *et al.*, in *Proceedings of the 3rd International Colloquium on X-ray Lasers, Schliersee, Germany, 1992*, edited by E. Fill, IOP Conf. Proc. No. 125 (Institute of Physics and Physical Society, London, 1992), Sec. 6, p. 309.
[31] P. Mandelbaum, M. Finkenthal, E. Meroz, J. Schwob, J. Oreg, W. Goldstein, M. Klapisch, A. Osterheld, A. Bar-Shalom, S. Lippmann, L. Huang, and H. W. Moos, Phys. Rev. A **42**, 4412 (1990).
[32] J. Oreg, W. Goldstein, P. Mandelbaum, D. Mitnik, E. Meroz, J. Schwob, and A. Bar-Shalom, Phys. Rev. A **44**, 1741 (1991).
[33] J. Oreg, W. Goldstein, M. Klapisch, and A. Bar-Shalom, Phys. Rev. A **44**, 1750 (1991).
[34] D. Mitnik, P. Mandelbaum, J. Schwob, A. Bar-Shalom, J. Oreg, and W. H. Goldstein, Phys. Rev. A **50**, 4911 (1994).

[35] M. Klapisch, J. Schwob, B. Fraenkel, and J. Oreg, J. Opt. Soc. Am. **67**, 148 (1977); M. Klapisch, Comput. Phys. Commun. **2**, 239 (1971).
[36] W. H. Goldstein, A. L. Osterheld, J. Oreg, and A. Bar-Shalom, Astrophys. J. Lett. **344**, L37 (1989).
[37] A. Bar-Shalom, M. Klapisch, and J. Oreg, Phys. Rev. A **38**, 1773 (1988).
[38] J. E. Rice, K. B. Fournier, M. A. Graf, J. L. Terry, M. Finkenthal, F. Bombarda, E. S. Marmar, and W. H. Goldstein, Phys. Rev. A **51**, 3551 (1995).
[39] R. D. Cowan, *The Theory of Atomic Structure and Spectra* (University of California Press, Berkeley, 1981), pp. 438–440.
[40] W. H. Hill, B. P. Flannery, S. A. Teukolsky, and W. T. Vetterling, *Numerical Recipes* (Cambridge University Press, Cambridge, England, 1986), p. 523.